Inorganic Chemistry

ARTICLE

pubs.acs.org/IC

Phosphorescent Iridium(III) Complex with an N^O Ligand as a Hg^{2+}-Selective Chemodosimeter and Logic Gate

Yi Liu,[†] Meiyi Li,[†] Qiang Zhao,[‡] Huazhou Wu,[†] Kewei Huang,[†] and Fuyou Li*[,†]

[†]Department of Chemistry, Fudan University, Shanghai, 200433, P.R. China

[‡]Key Laboratory for Organic Electronics & Information Displays (KLOEID) and Institute of Advanced Materials (IAM), Nanjing University of Posts and Telecommunications, Nanjing, 210046, P.R. China

Supporting Information

ABSTRACT: Phosphorescent iridium(III) complexes have been attracting increasing attention in applications as luminescent chemosensors. However, no instance of an iridium(III) complex being used as a molecular logic gate has hitherto been reported. In the present study, two iridium(III) complexes, $[Ir(ppy)_2(PBT)]$ and $[Ir(ppy)_2(PBO)]$, have been synthesized (PBT, 2-(2-Hydroxyphenyl)-benzothiazole; PBO, 2-(2-hydroxyphenyl)-benzoxazole), and their chemical structures have been characterized by single-crystal X-ray analysis. Theoretical calculations and detailed studies of the photophysical and electrochemical properties of these two complexes have shown that the N^O ligands dominate their luminescence emission properties. Moreover, $[Ir(ppy)_2(PBT)]$, containing a sulfur atom in the N^O ligand, can serve as a highly selective chemodosimeter for Hg^{2+} with ratiometric and naked-eye detection, which is associated with the dissociation of the N^O ligand PBT from the complex. Furthermore, complex $[Ir(ppy)_2(PBT)]$ has been further developed as an AND and INHIBIT logic gate with Hg^{2+} and histidine as inputs.

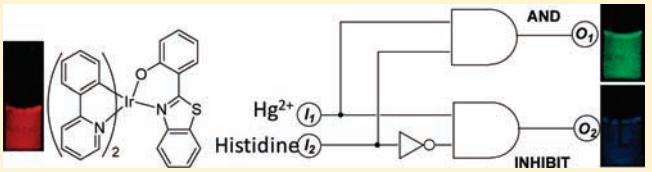

INTRODUCTION

Phosphorescent iridium(III) complexes have been attracting considerable attention as a class of excellent phosphorescent materials, because of their advantageous photophysical properties, such as high phosphorescent quantum yields at room temperature, tunable emission wavelength through the modification of ligand structures, and long-lived excited states.[1] Hence, phosphorescent iridium(III) complexes have been applied successfully in many optoelectronic devices, such as organic light-emitting diodes (OLEDs),[2] light-emitting electrochemical cells,[3] and molecular devices (such as chemosensor,[4] biological labeling reagents,[5,6] and bioimaging probes[7]).

Recently, the application of phosphorescent iridium(III) complexes as molecular probes in molecular devices has attracted increasing interest, as a result of their excellent emission properties compared with those of purely organic luminophores.[8] For example, we and other groups have exploited a series of excellent phosphorescent probes based on iridium(III) complexes for anions,[9] metal cations,[10] amino acids,[11] and biomolecules.[12] Lo's group and our group developed a series of phosphorescent iridium(III) complexes for cell imaging, and investigated the relationship between their chemical structures and cell uptake behaviors.[13,14] In addition, phosphorescent iridium(III) complexes for monitoring intracellular cysteine and homocysteine have been reported by our group.[11b]

As an important constituent of molecular computers, molecular logic gates for converting chemical, electrical, and optical inputs into the detectable outputs has become an active research area in material science. Recently, a number of fluorescent probes based on organic dyes have been developed as molecular logic gates.[15,16] For example, Tian et al. reported that the characteristic fluorescence of Hg^{2+}-selective OFF-ON and Cu^{2+}-selective ON-OFF operations could be monitored and reversibly controlled by the sequence and ratio of Hg^{2+} and Cu^{2+} inputs to construct a crossword puzzle and a logic memory at the molecular level.[15c] However, few works on molecular logic gates based on phosphorescence signals have been reported to date, although phosphorescence measurements have some unique advantages compared with the fluorescence signals of organic dyes. Hence, the construction of molecular logic gates with phosphorescence signals based on the developed phosphorescent complexes should prove to be an interesting topic.

On the basis of the above considerations, in the present study we have designed and synthesized a neutral iridium(III) complex, $[Ir(ppy)_2(PBT)]$, PBT = 2-(2-hydroxyphenyl)-benzothiazole, as a phosphorescent chemodosimeter for Hg^{2+} and a molecular logic gate. In our design strategy, the interaction of Hg^{2+} with the S atom in the PBT [2-(2-Hydroxyphenyl)-benzothiazole] ligand can induce the dissociation of this ligand from the complex $[Ir(ppy)_2(PBT)]$, thereby affecting its luminescence emission properties, which provides a means of detecting Hg^{2+}. Further addition of histidine induces a spectral shift of the phosphorescence signal, thereby realizing an AND and INHIBIT logic gate

Received: December 12, 2010
Published: June 03, 2011

Scheme 1. Chemical Structure of Ir(ppy)$_2$(PBT) (1) and Ir(ppy)$_2$(PBO) (2)

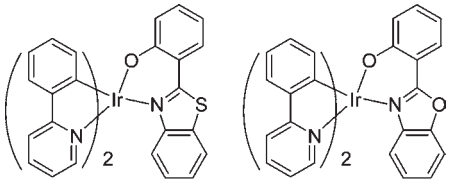

Ir(ppy)$_2$(PBT) 1 Ir(ppy)$_2$(PBO) 2

with Hg^{2+} and histidine as two inputs and phosphorescence as the output signal. The photophysical properties and recognition behaviors of [Ir(ppy)$_2$(PBT)] have been investigated in detail through UV/vis absorption spectra, luminescence spectra, cyclic voltammetry, and theoretical calculations. For comparison, another iridium complex, [Ir(ppy)$_2$(PBO)], PBO = 2-(2-hydroxyphenyl)-benzoxazole, has also been investigated (Scheme 1).

EXPERIMENTAL SECTION

Materials. PBT, PBO, and 2-phenylpyridine (ppy) were purchased from Acros Organics. Mercury(II) perchlorate hydrate ($Hg(ClO_4)_2 \cdot 3H_2O$) and histidine (His) were purchased from Aldrich. Iridium(III) trichloride hydrate ($IrCl_3 \cdot 3H_2O$) and other chemicals were purchased from China Pharmaceutical Co. Ltd. and used without further purification.

Synthesis of Ir(ppy)$_2$(PBT). A mixture of 2-ethoxyethanol and water (3:1, v/v) was added to a flask containing $IrCl_3 \cdot 3H_2O$ (1.0 mmol) and 2-phenylpyridine (2.5 mmol). The mixture was refluxed for 24 h. After cooling, the yellow solid precipitate was filtered to give crude cyclometalated Ir(III) chloro-bridged dimer. The chloro-bridged dimer (0.2 mmol), Na_2CO_3 (1.4 mmol) and 2-ethoxyethanol/H_2O (40 mL, 1:1, v/v) were added to the flask. 2-(2-Hydroxyphenyl)-benzothiazole (0.5 mmol) was added slowly and then the mixture was heated to 110 °C for 12 h under N_2 atmosphere. After cooling to room temperature, the red precipitate was collected by filtration and purified by silica gel chromatograph using CH_2Cl_2/MeOH (100:1, v/v) to afford the red complex Ir(ppy)$_2$(PBT) in yield 61%. mp 341−343 °C; ^{1}H NMR (500 MHz, d_8-THF) δ 9.01 (d, J = 4.9 Hz, 1H), 8.24 (d, J = 5.8 Hz, 1H), 7.96 (d, J = 8.1 Hz, 1H), 7.91 (d, J = 8.0 Hz, 1H), 7.73−7.64 (m, 4H), 7.54 (d, J = 6.6 Hz, 1H), 7.49−7.47 (m, 1H), 7.20 (d, J = 8.5 Hz, 1H), 7.06−7.04 (m, 2H), 6.95−6.87 (m, 1H), 6.90−6.85 (m, 1H), 6.77−6.74 (m, 3H), 6.62−6.58 (m, 1H), 6.58−6.55 (m, 1H), 6.45−6.43 (m, 1H), 6.40−6.38 (m, 1H), 6.27−6.24 (m, 1H), 5.94−5.92 (m, 1H); MS-(ESI-MS): calcd. for $C_{35}H_{24}IrN_3OS$ 727.1 $[M]^+$; found 728.1 $[M+H]^+$.

Synthesis of Ir(ppy)$_2$(PBO). The procedure for the synthesis of Ir(ppy)$_2$(PBO) was similar to that for Ir(ppy)$_2$(PBT), and a yellow complex Ir(ppy)$_2$(PBO) was obtained in yield 59%. mp 338−340 °C; ^{1}H NMR (500 MHz, $CDCl_3$) δ 8.87 (d, J = 5.1 Hz, 1H), 8.12 (d, J = 5.1 Hz, 1H), 7.99−7.96 (m, 1H), 7.88−7.86 (d, J = 8.1 Hz, 1H), 7.79−7.77 (m, J = 8.1 Hz, 1H), 7.67−7.59 (m, 4H), 7.44−7.42 (d, J = 8.1 Hz, 1H), 7.24−7.16(m, 1H), 7.13−7.09(m, 1H), 7.05−7.02 (m, 1H), 6.95−6.92 (m, 1H), 6.91−6.88 (m, 1H), 6.87−6.84 (m, 1H), 6.83−6.80 (m, 1H), 6.79−6.75 (m, 3H), 6.69−6.65 (m, 1H), 6.49−6.45 (m, 1H), 6.21−6.19 (m, 1H), 6.08−6.06 (m, 1H); MS(ESI-MS): calcd. for $C_{35}H_{24}IrN_3O_2$ 711.2 $[M]^+$; found 712.2 $[M+H]^+$.

General Experiments. All reactions were performed under nitrogen atmosphere. The ^{1}H NMR spectra of Ir(ppy)$_2$(PBT) and Ir(ppy)$_2$-(PBO) in d_8-THF or $CDCl_3$ were recorded on a Bruker spectrometer at 500 MHz. Electrospray ionization mass spectra (ESI-MS) were measured on a Micromass LCTTM system. The UV−visible absorption spectra were recorded on a Shimadzu UV-2550 spectrometer. Steady-state emission spectra of Ir(ppy)$_2$(PBT) and Ir(ppy)$_2$(PBO) at room temperature were measured on an Edinburgh instrument LP-920 spectrometer. The luminescence quantum yields of Ir(ppy)$_2$(PBT) and Ir(ppy)$_2$(PBO) in CH_2Cl_2 solution was measured with reference to ruthenium(II) complex $Ru(bpy)_3^{2+}$ (Φ_f = 0.028 in water). Lifetime studies were performed with an Edinburgh FL-920 photocounting system with a hydrogen-filled flashlamp as the excitation source. The data were analyzed by iterative convolution of the luminescence decay profile with the instrument response function using a software package provided by Edinburgh Instruments. Samples for absorption and emission measurements were contained in quartzose-cuvettes (1 cm ×1 cm). Deionized water was used to prepare all metal cation aqueous solutions.

Theoretical Calculations. The geometric and energy optimizations were performed with the Gaussian 03 program based on the density functional theory (DFT) method.[17] Becke's three parameter hybrid functional with the Lee−Yang−Parr correlation functional (B3LYP) was employed for all the calculations. The LANL2DZ basis set was used to treat the iridium atom, whereas the 3-21G* basis set was used to treat all other atoms. Once an optimized geometry was obtained, imaginary frequencies were checked at the same level by vibration analysis to verify the genuine minimum on the potential energy surfaces (PES). To understand the nature of the excited state, the orbital analyses of the complexes were also performed.

Electrochemical Measurements. Electrochemical measurements were performed with an Eco Chemie Autolab. All measurements were carried out in a one-compartment cell under N_2 atmosphere, equipped with a glassy-carbon working electrode, a platinum wire counter electrode, and an Ag/Ag^+ reference electrode. The supporting electrolyte was a 0.10 $mol \cdot L^{-1}$ CH_2Cl_2 solution of tetrabutylammonium hexafluorophosphate (Bu_4NPF_6). The ferrocene/ferrocenium couple was added and used as the internal standard. The scan rate was 50 $mV \cdot s^{-1}$.

X-ray Crystallography Analysis of Ir(ppy)$_2$(PBT) and Ir-(ppy)$_2$(PBO). The single crystal was mounted on a glass fiber and transferred to a Bruker SMART CCD. Crystallographic measurement was carried out using a Bruker SMART CCD diffractometer, σ scans, and graphite monochromated Mo Kα radiation (λ = 0.71073 Å) at room temperature. The structure was solved by direct methods and refined by full-matrix least-squared on F^2 using the program SHELXS-97. All non-hydrogen atoms were refined anisotropically. Hydrogen atoms were calculated in ideal geometries. For the full matrix least-squares refinements [$I > 2\sigma(I)$], the unweighted and weighted agreement factors of $R1 = \Sigma||F_o| - |F_c||/\Sigma|F_o|$ and $wR2 = [\Sigma w(F_o^2 - F_c^2)^2/\Sigma w(F_o^4)]^{1/2}$ were used. Cambridge Crystallographic Data Centre (CCDC) numbers of Ir(ppy)$_2$(PBT) and Ir(ppy)$_2$(PBO) are 699179 and 709611, respectively.

RESULTS AND DISCUSSION

Synthesis of Complexes. The synthetic procedure for complexes Ir(ppy)$_2$(PBT) and Ir(ppy)$_2$(PBO) includes two steps. First, the chloro-bridged dinuclear cyclometalated iridium(III) precursor $[Ir(ppy)_2Cl]_2$ was synthesized by the same method as reported by Nonoyama.[18] And then the iridium(III) complexes were synthesized by the bridged-splitting reactions of crude $[Ir(ppy)_2Cl]_2$ and subsequent complexation with N^O ligand PBT and PBO. Both the complexes Ir(ppy)$_2$(PBT) and Ir(ppy)$_2$-(PBO) were obtained in good yields. Their structures were characterized by ^{1}H NMR, ESI-MS, and X-ray crystallography.

Single Crystal Structures of Ir(ppy)$_2$(PBT) and Ir(ppy)$_2$-(PBO). The single crystal of Ir(ppy)$_2$(PBT) was obtained from the mixed solution of dichloromethane and ether, and that of Ir(ppy)$_2$(PBO) was obtained by the slow evaporation of

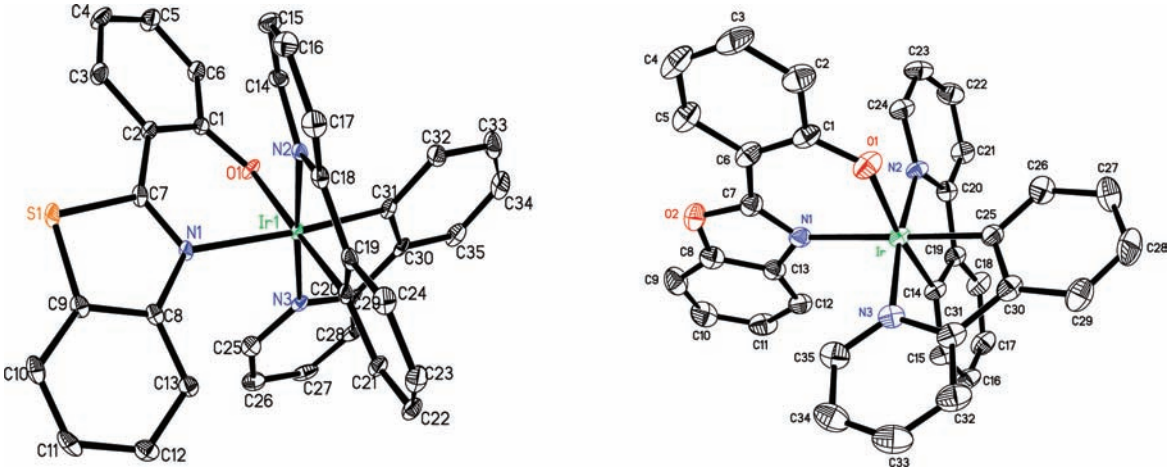

Figure 1. Crystal structures of $Ir(ppy)_2(PBT)$ (left) and $Ir(ppy)_2(PBO)$ (right) with thermal ellipsoids are drawn at the 40% probability level, and the H atoms and solvent molecules have been omitted for clarity.

dichloromethane into the acetonitrile solution. Figure 1 shows the crystal structures of $Ir(ppy)_2(PBT)$ and $Ir(ppy)_2(PBO)$. The crystallographic refinement parameters of $Ir(ppy)_2(PBT)$ and $Ir(ppy)_2(PBO)$ are summarized in Table 1, and the selected relevant bond length (Å) and bond angle (deg) parameters are listed in Supporting Information, Table S1 and S2.

The iridium(III) centers in both complexes $Ir(ppy)_2(PBT)$ and $Ir(ppy)_2(PBO)$ adopt a distorted octahedral coordination geometry with cis metalated carbons and trans nitrogen atoms, as revealed by previous structural studies on mononuclear species containing the cyclometalated C^N ligands.[19] Compared with $[Ir(ppy)_2(PBO)]$, $[Ir(ppy)_2(PBT)]$ shows slightly longer Ir−C, Ir−N, and Ir−O bond lengths, as shown in the Supporting Information, Tables S1 and S2, indicating that it is somewhat less stable. In both $[Ir(ppy)_2(PBT)]$ and $[Ir(ppy)_2(PBO)]$, both the $Ir-N_{(N^O)}$ (~2.18 Å) and Ir−O (~2.13 Å) bond lengths are significantly longer than that of $Ir-N_{(C^N)}$ (~2.04 Å). In particular, the $Ir-N_{(N^O)}$ and Ir−O distances in $[Ir(ppy)_2(PBT)]$ are 2.204(3) and 2.143(2) Á, respectively, which are longer than those in $[Ir(ppy)_2(PBO)]$. These facts suggest that the N^O ligand PBT may be easily dissociated from $[Ir(ppy)_2(PBT)]$ than $[Ir(ppy)_2(PBO)]$. In addition, it can be seen from Supporting Information, Tables S1 and S2 that the $N_{(N^O)}-Ir-O_{(N^O)}$, $N_{(CN)}-Ir-O_{(N^O)}$, and $N_{(C^N)}-Ir-N_{(N^O)}$ bite angles are very different for $[Ir(ppy)_2(PBT)]$ and $[Ir(ppy)_2(PBO)]$, which indicates that the N^O ligands have a significant effect on the structures of the complexes.

Absorption Spectroscopy. The UV−vis absorption spectra of the two complexes were measured in CH_2Cl_2 solutions at 298 K (Figure 2). The relevant data are collected in Table 2. Both of the two complexes display intense absorption bands below 350 nm with an extinction coefficient ε of $\sim 10^5$ $mol^{-1}\cdot L\cdot cm^{-1}$, which are assigned to the spin-allowed singlet ligand-centered LC ($\pi-\pi^*$) transitions. The weak absorption bands in the range of 350−500 nm with an extinction coefficient ε of $\sim 10^3$ $mol^{-1}\cdot L\cdot cm^{-1}$ are assigned to the metal-to-ligand charge transfer (MLCT) and ligand-to-ligand charge transfer (LLCT) transitions. Interestingly, the absorption band of $Ir(ppy)_2(PBT)$ is red-shifted evidently in comparison with that of $Ir(ppy)_2(PBO)$, indicating that the N^O ligand influences the ground-state electronic structures and photophysical properties of complexes.

Table 1. Crystallographic Data for $Ir(ppy)_2(PBT)$ and $Ir(ppy)_2(PBO)$

	$Ir(ppy)_2(PBT)$	$Ir(ppy)_2(PBO)\cdot CH_3CN$
chemical formula	$C_{35}H_{24}IrN_3OS$	$C_{37}H_{27}IrN_4O_2$
Fw	726.83	751.83
cryst syst	triclinic	triclinic
space group	$P\bar{1}$	$P1$
a (Å)	10.8920(12)	8.9186(9)
b (Å)	11.6541(14)	10.4896(10)
c (Å)	12.0711(16)	16.9431(16)
α (deg)	75.631(8)	103.388(2)
β (deg)	68.776(7)	97.092(2)
γ (deg)	71.478(8)	106.612(2)
V	1338.9(3)	1446.7(2)
Z	2	2
T (K)	113(2)	293(2)
D_{calcd} ($g\cdot cm^{-3}$)	1.803	1.726
μ (mm^{-1})	5.100	4.657
$2\theta_{max}$ (deg)	52.06	51.48
no. of reflns collected	11655	8596
no. of unique reflns	6297	6140
no. of obsd reflns	5554	5515
no. of variables	370	399
R	0.0304	0.0353
wR	0.0702	0.0819
GOF	1.018	1.036

Luminescence Spectroscopy. The room-temperature photoluminescence spectra of two complexes in dichloromethane solutions and solid state are shown in the Figure 2. In CH_2Cl_2 solution, both $Ir(ppy)_2(PBT)$ and $Ir(ppy)_2(PBO)$ display structureless emission bands with maximal wavelength at 602 and 523 nm with quantum efficiency of 1.8% and 0.68%, respectively. The emission lifetimes measured in an air-equilibrated solution at room temperature are 0.98 and 1.73 μs for $Ir(ppy)_2(PBT)$ and $Ir(ppy)_2(PBO)$, respectively. Such long-lived excited states indicate that the emitting states of the two iridium(III) complexes have triplet character. Moreover, the

dx.doi.org/10.1021/ic102481x |*Inorg. Chem.* 2011, 50, 5969–5977

photoluminescence spectra of $Ir(ppy)_2(PBT)$ and $Ir(ppy)_2(PBO)$ are broad and featureless, indicating that the emission originates primarily from the triplet ^3CT excited states. Interestingly, compared with $Ir(ppy)_2(PBO)$, $Ir(ppy)_2(PBT)$ exhibited a significant red-shift of 80 nm in the emission wavelength, corresponding to the change of emission color from green to red by changing the N^O ligand from PBO to PBT. Considering that both complexes have the same C^N ligand, it can be deduced that the different emission properties for $Ir(ppy)_2(PBT)$ and $Ir(ppy)_2(PBO)$ are associated with the difference of the S and O atoms in the N^O ligands. Thus, through changing the N^O ligands, the emission wavelengths and colors were tuned significantly.

Electrochemical Properties. The electrochemical properties of $Ir(ppy)_2(PBT)$ and $Ir(ppy)_2(PBO)$ were studied by cyclic voltammetry (CV) in CH_2Cl_2 solution.[20] The data are listed in Table 2. Complexes $Ir(ppy)_2(PBT)$ and $Ir(ppy)_2(PBO)$ exhibited the irreversible oxidation wave at 0.90 and 0.96 V, respectively. It is assumed that pure metal-centered oxidation is reversible, and the irreversibility increases as the contribution to the highest occupied molecular orbital (HOMO) of the N^O ligands increases. Therefore, the irreversible oxidation process could be assigned to orbitals receiving strong contributions from the iridium center and the $Ir-O^-$ σ-bond orbitals simultaneously. Complexes $Ir(ppy)_2(PBT)$ and $Ir(ppy)_2(PBO)$ exhibited the irreversible reduction wave at -1.86 and -1.84 V, respectively. In addition, the similar second reduction potential for both complexes is assigned to the reduction of the C^N ligand (ppy), and this potential is also similar to that in the previous report.[21]

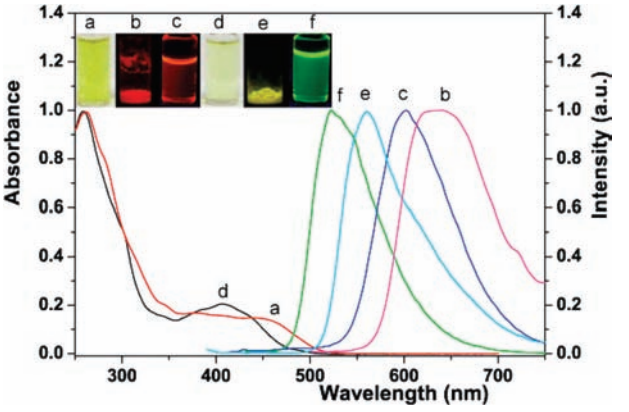

Figure 2. Absorption, emission spectra and colors of $Ir(ppy)_2(PBT)$ and $Ir(ppy)_2(PBO)$ in different condition. Inset: (a–e) Photos of two samples $Ir(ppy)_2(PBT)$ and $Ir(ppy)_2(PBO)$ in different states. (a, d) bright-field photo of $Ir(ppy)_2(PBT)$ (a) and $Ir(ppy)_2(PBO)$ (b) in CH_2Cl_2 (200 μM) solution; (b, c) emission photos of $Ir(ppy)_2(PBT)$ in powder (b) and in CH_2Cl_2 solution (c); (e, f) emission photos of $Ir(ppy)_2(PBO)$ in powder (e) and in CH_2Cl_2 solution (f).

Theoretical Calculations. To further investigate the nature of the excited states, DFT and time-dependent DFT (TDDFT) calculations were performed for $[Ir(ppy)_2(PBT)]$ and $[Ir(ppy)_2(PBO)]$. The calculated distributions of molecular orbitals (HOMO-2, HOMO-1, HOMO, LUMO, LUMO+1, and LUMO+2) are shown in Table 3, and the calculated low-energy singlet- and triplet-state transitions of $[Ir(ppy)_2(PBT)]$ and $[Ir(ppy)_2(PBO)]$ are shown in Table 4. The HOMO of $[Ir(ppy)_2(PBT)]$ primarily resides on the iridium center with a small distribution on the phenyl group of the N^O ligand. Its lowest unoccupied molecular orbital (LUMO) is distributed over the whole N^O ligand. For the complex $[Ir(ppy)_2(PBO)]$, both the iridium center and the phenyl group of the N^O ligand contribute to the HOMO. The LUMO of $[Ir(ppy)_2(PBO)]$ is mainly located on the C^N ligand.

According to the calculated oscillator strength, the lowest singlet transition responsible for the measured low-energy absorption band of $[Ir(ppy)_2(PBT)]$ at 452 nm is assigned to the S_1 state (478 nm), which is mainly composed of the HOMO→LUMO transition. The calculated energy of the absorption band is very similar to the experimental data. According to the orbital distributions, this absorption band is mainly assigned to the $[d\pi(Ir)\rightarrow\pi^*_{N^O}]$ MLCT transition, with a small contribution from the LC $(\pi-\pi^*)_{N^O}$ transition. That is to say, the N^O ligand PBT dominates the transitions. However, for $[Ir(ppy)_2(PBO)]$, the S_2 state (433 nm) is responsible for the

Table 2. Photophysical Parameters and Electrochemical Data for $Ir(ppy)_2PBT$ (1) and $Ir(ppy)_2PBO$ (2)

	λ_{abs}, nm[a]	τ, μs[a]	λ_{em}, nm[a]	τ, μs[a]	Φ_f[b], %	E_a^{ox}, V	E_{onset}^{ox}, V	$E_{1/2}^{re}$ or E_c^{re}, V	E_{onset}^{re}, V
1	260,452	0.98	602	0.98	1.8	0.90	0.74	−1.18[c], −1.86[c]	−0.69
2	259,407	1.73	523	1.73	0.68	0.96	0.82	−1.19[c], −1.84[c]	−0.77

[a] Measured in CH_2Cl_2 solution. Concentration: 20 μM, T = 298K. [b] Reference to ruthenium(II) complex $Ru(bpy)_3^{2+}$. [c] Irreversible wave.

Table 3. Selected Frontier Orbitals of Complex $Ir(ppy)_2PBT$ and $Ir(ppy)_2PBO$

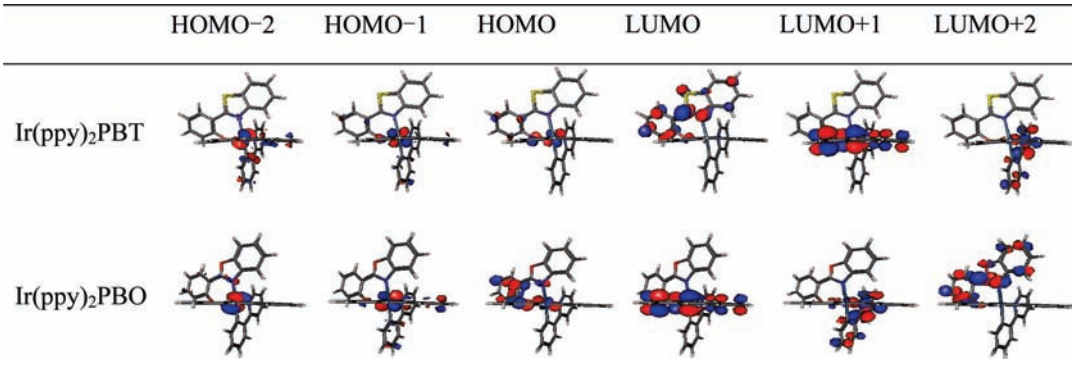

dx.doi.org/10.1021/ic102481x |Inorg. Chem. 2011, 50, 5969–5977

Table 4. Calculated Energy Levels of the Lower Lying Transitions of Complex 1 and 2

		assignment					
	state	from	to	coefficient	energy (eV)	wavelength (nm)	oscillator strength
1	S_1	HOMO	LUMO	69%	2.595	477.7	0.0332
		HOMO	LUMO+1	17%			
		HOMO	LUMO+2	5%			
	S_2	HOMO	LUMO	6%	2.681	462.5	0.0144
		HOMO	LUMO+1	62%			
		HOMO	LUMO+2	25%			
	S_3	HOMO-1	LUMO+2	3%	2.721	455.0	0.0199
		HOMO	LUMO	14%			
		HOMO	LUMO+1	13%			
		HOMO	LUMO+2	63%			
	S_4	HOMO-1	LUMO	66%	2.998	413.6	0.0432
		HOMO-1	LUMO+1	25%			
	S_5	HOMO-1	LUMO	23%	3.040	407.8	0.0219
		HOMO-1	LUMO+1	67%			
	T_1	HOMO-1	LUMO	11%	2.109	587.9	0
		HOMO	LUMO	85%			
		HOMO	LUMO+2	3%			
2	S_1	HOMO-1	LUMO	11%	2.772	447.3	0.0061
		HOMO	LUMO	83%			
		HOMO	LUMO+1	2%			
	S_2	HOMO-1	LUMO	62%	2.863	433.1	0.0311
		HOMO-1	LUMO+1	5%			
		HOMO	LUMO	5%			
		HOMO	LUMO+1	22%			
	S_3	HOMO-1	LUMO	12%	2.869	432.1	0.0102
		HOMO-1	LUMO+1	6%			
		HOMO	LUMO	7%			
		HOMO	LUMO+1	72%			
	S_4	HOMO-1	LUMO	8%	2.912	425.8	0.0005
		HOMO-1	LUMO+1	83%			
	S_5	HOMO-1	LUMO+2	10%	2.980	416.1	0.0788
		HOMO	LUMO+2	79%			
		HOMO-1	LUMO+4	89%			
	T_1	HOMO-1	LUMO+2	3%	2.332	531.6	0
		HOMO	LUMO+2	97%			

experimentally observed low-energy absorption band (407 nm) according to the calculated oscillator strength, which is also assigned to the HOMO→LUMO transition.

According to the orbital distributions, $[d\pi(Ir)\rightarrow\pi^*_{C\hat{}N}]$ MLCT and $[\pi_{N\hat{}O}\rightarrow\pi^*_{C\hat{}N}]$ intraligand charge-transfer (ILCT) transitions are responsible for the absorption band at 433 nm, that is to say, the C^N ligand dominates the absorption band, which is different from the situation in $[Ir(ppy)_2(PBT)]$. The lowest triplet states (T_1) of $[Ir(ppy)_2(PBT)]$ and $[Ir(ppy)_2(PBO)]$ originate from the HOMO→LUMO and HOMO →LUMO+2 transitions, respectively. The calculated emission wavelengths for $[Ir(ppy)_2(PBT)]$ and $[Ir(ppy)_2(PBO)]$ are 588 and 532 nm, respectively, which are also very close to the experimental data. According to the orbital distributions, both the $[d\pi(Ir)\rightarrow\pi^*_{N\hat{}O}]$ MLCT and the LC $(\pi-\pi^*)_{N\hat{}O}$ transitions are responsible for the excited states of $[Ir(ppy)_2(PBT)]$ and $[Ir(ppy)_2(PBO)]$. In addition, the $[\pi_{C\hat{}N}\rightarrow\pi^*_{N\hat{}O}]$ LLCT transition also makes some contribution to the excited state of $[Ir(ppy)_2(PBO)]$. Hence, we can conclude that the N^O ligands dominate the emission properties of these two complexes and that the different electronic properties of the sulfur and oxygen atoms result in the significantly different emission wavelengths.

Optical Response of $[Ir(ppy)_2(PBT)]$ to Hg^{2+}. In view of the dependence of the luminescence of $[Ir(ppy)_2(PBT)]$ on the ligand PBT and the potential interaction[22] between Hg^{2+} and the sulfur atom of PBT, it is reasonable to expect that $[Ir(ppy)_2(PBT)]$ might be used for the selective detection of Hg^{2+}. In the present study, the sensing ability of $[Ir(ppy)_2(PBT)]$ has been investigated through UV/vis absorption and photoluminescence techniques.

Considering the significance of detection in aqueous media, an optimized solvent system of THF/H_2O (1:9, v/v) was selected for the spectroscopic investigation. The luminescence and absorption spectra of $[Ir(ppy)_2(PBT)]$ in the absence and presence

dx.doi.org/10.1021/ic102481x |Inorg. Chem. 2011, 50, 5969–5977

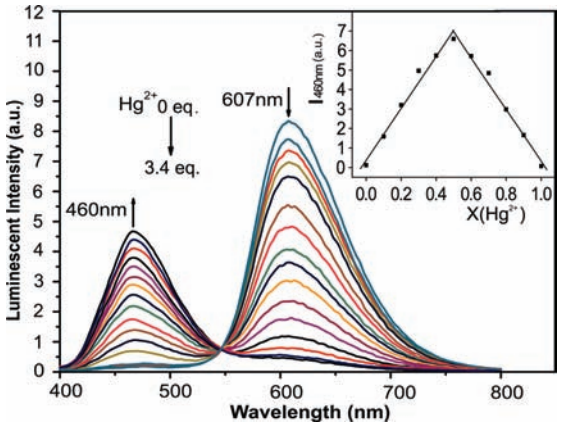

Figure 3. Luminescent response of $Ir(ppy)_2(PBT)$ (2×10^{-5} M) in solution (THF/H_2O, 1:9, v/v) to Hg^{2+} (0.1 M, 3.4 equiv.) under excitation at 360 nm.

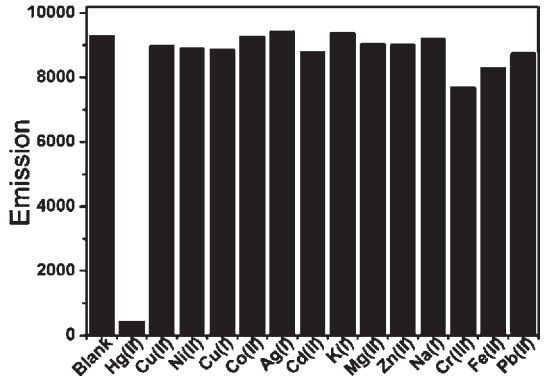

Figure 4. Luminescent responses of $Ir(ppy)_2(PBT)$ (50 μM) in THF/H_2O (1:9) to various metal ions (5.0 equiv) at 25 °C.

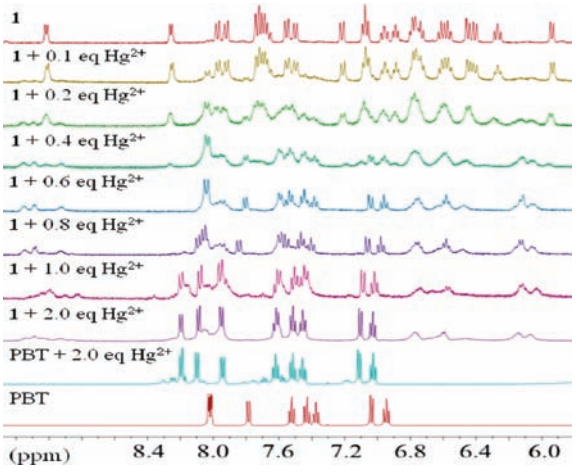

Figure 5. ^1H NMR spectra between ligand PBT and $Ir(ppy)_2(PBT)$ (**1**) with Hg^{2+} in d_8-THF. (a) only PBT; (b) only $Ir(ppy)_2(PBT)$; (c) PBT with 2.0 equiv of Hg^{2+}; (d) $Ir(ppy)_2(PBT)$ with 2.0 equiv of Hg^{2+}.

of Hg^{2+} are shown in Figure 3 and Supporting Information, Figure S8, respectively. The addition of increasing amounts of Hg^{2+} to a solution of $[Ir(ppy)_2(PBT)]$ induced some changes in its absorption spectrum. The absorbance at 452 nm gradually decreased, which led to an evident color change from orange to colorless. This indicated a strong interaction between $[Ir(ppy)_2(PBT)]$ and Hg^{2+}.

In THF/H_2O (1:9, v/v) solution, $[Ir(ppy)_2(PBT)]$ shows an intense emission band at 607 nm, and the photoluminescence color is red (Figure 2 inset). Upon excitation at 360 nm, the emission intensity at 607 nm decreased and a new band gradually appeared at 460 nm when Hg^{2+} was added into the solution of $[Ir(ppy)_2(PBT)]$, corresponding to a significant blue-shift of 147 nm with an isoemissive point at 545 nm. As a result, the emission color was distinctively changed from red to blue, which could be observed by the naked eye. The large difference between the two emission wavelengths (147 nm) is very beneficial for the accurate measurement of the two emission intensities. In addition, the ratio of the emission intensities at 460 and 607 nm (I_{607}/I_{460}) undergoes a dramatic change from 38.96 to 0.08 upon the addition of Hg^{2+} (Supporting Information, Figure S9). Such a large change in the ratio of the emission intensities at the two wavelengths indicates that $[Ir(ppy)_2(PBT)]$ is capable of serving as a ratiometric phosphorescent probe for Hg^{2+}. At the concentration of $[Ir(ppy)_2(PBT)]$ used in this study, Hg^{2+} could be detected down to a concentration of 10^{-7} mol·L^{-1}, namely, in the parts per billion (ppb) range. In addition, a Job's plot analysis showed that the binding stoichiometry was 1:1 in CH_3CN solution (Figure 3 inset). Interestingly, under excitation at 460 nm, the phosphorescent emission of $[Ir(ppy)_2(PBT)]$ at 607 nm was quenched, and no short-wavelength emission was observed (Supporting Information, Figure S10), which is significantly different from the case excited at 365 nm. In addition, no change in emission of $[Ir(ppy)_2(PBO)]$ was observed upon addition of Hg^{2+}. These facts indicate a strong interaction between the sulfur atom of $[Ir(ppy)_2(PBT)]$ and Hg^{2+}.

Selective Optical Response of Complex Ir(ppy)$_2$(PBT) to Various Metal Ions. For an excellent chemosensor, high selectivity is very important. To validate the selectivity of $Ir(ppy)_2(PBT)$, some other metal ions including some alkali (Na^+, K^+), alkaline earth (Mg^{2+}), and transition metal ions (Cu^{2+}, Ni^{2+}, Cu^+, Co^{2+}, Ag^+, Cd^{2+}, Cr^{3+}, Fe^{2+}, Pb^{2+}) were tested under the same condition as that of Hg^{2+} by absorption and luminescent spectroscopy. As shown in Figure 4, only the addition of Hg^{2+} resulted in a prominent emission change, whereas very weak variations were observed upon addition of an excess of others metals ions. The results indicated that the $Ir(ppy)_2(PBT)$ can serve as a sensitive phosphorescent indicator for Hg^{2+}.

Mechanism of the Sensing of Hg^{2+} by [Ir(ppy)$_2$(PBT)]. In terms of Pearson's hard−soft acid−base theory,[23] Hg^{2+} is a soft ion (soft acid) and can interact preferentially with sulfur (a soft base). Herein, the interaction of $[Ir(ppy)_2(PBT)]$ with Hg^{2+} was further investigated by ^1H NMR and MS spectra technique. As shown in Figure 5, the chemical shifts of $[Ir(ppy)_2(PBT)]$ changed significantly upon addition of Hg^{2+}. When the amount of added Hg^{2+} ions reached 1.0 equivalent, the original peaks (Figure 5) of $[Ir(ppy)_2(PBT)]$ had disappeared, and the final spectrum in the presence of 2.0 equiv of Hg^{2+} was similar to that of a mixture of ligand PBT and 2.0 equiv of Hg^{2+} ions (Figure 5). This suggests that the interaction between $[Ir(ppy)_2(PBT)]$ and Hg^{2+} ions releases the ligand PBT to bind with Hg^{2+} and then a new complex is formed (Scheme 2A) in what constitutes a chemical reaction. This mechanism was further confirmed by ESI-MS measurements on a mixture of $[Ir(ppy)_2(PBT)]$ and 2.0 equiv of Hg^{2+}. As shown in the Supporting Information, Figure S12, the original peak at m/z 728.1 assigned to $[Ir(ppy)_2(PBT)]$

dx.doi.org/10.1021/ic102481x |*Inorg. Chem.* 2011, 50, 5969–5977

Scheme 2. Possible Mechanism of the Sensing Reaction

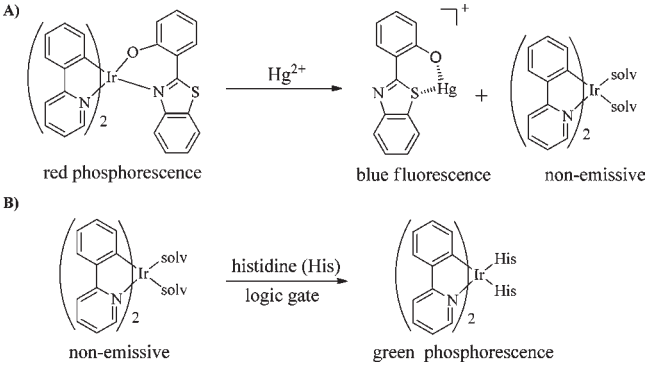

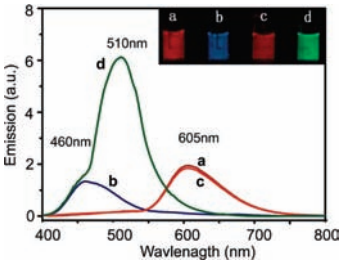

Figure 6. Luminescence spectra and emission photos (inset) of $[Ir(ppy)_2(PBT)]$ in the CH_3CN/H_2O (1:5, v/v) solution upon addition of Hg^{2+} and histidine. (a) only **1**; (b) **1** with 2.0 equiv of Hg^{2+}; (c) **1** with 5.0 equiv of histidine; (d) **1** with 2.0 equiv of Hg^{2+} and 5.0 equiv of histidine.

disappeared and a new peak was observed at m/z 534.9 attributable to $[Ir(ppy)_2(H_2O)_2]^+$. Moreover, the coordination interaction of the PBT ligand with Hg^{2+} ions was further confirmed by an obvious shift in the ^1H NMR signal of PBT upon addition of 2.0 equiv of Hg^{2+} (Supporting Information, Figure S4). According to the above analyses, we can conclude that upon bonding with Hg^{2+} the N^O ligand (PBT) dissociates from $[Ir(ppy)_2(PBT)]$ and the fragment $[Ir(ppy)_2]^+$ further combines with two H_2O molecules to form a new complex $[Ir(ppy)_2(H_2O)_2]^+$. Hence, such a probe for Hg^{2+} based on $[Ir(ppy)_2(PBT)]$ can be classed as a chemodosimeter.

Logic Gates Based on $[Ir(ppy)_2(PBT)]$ with Hg^{2+} and Histidine As Inputs. It has been reported that the formed Ir(III) solvent complex $[Ir(ppy)_2(H_2O)_2]^+$ is nonemissive, but may selectively bind histidine to form a luminescence-enhanced complex.[6] In the present study, the response of $[Ir(ppy)_2(PBT)]$ to histidine and/or Hg^{2+} has been investigated by luminescence analysis. As shown in Figure 6, when only histidine was added to a solution of $[Ir(ppy)_2(PBT)]$, the spectral change was very slight. However, upon addition of both histidine and Hg^{2+}, the luminescence spectrum of $[Ir(ppy)_2(PBT)]$ changed significantly, and a new peak at 510 nm was formed immediately, corresponding to an obvious change in the emission color from red to green. These facts indicated that the presence of Hg^{2+} promoted the interaction of $[Ir(ppy)_2(PBT)]$ with histidine. The process is shown schematically in Scheme 2.

Furthermore, the effects of Hg^{2+} ions and histidine on the luminescence of $[Ir(ppy)_2(PBT)]$ permit this complex to be fabricated as a more advanced and functional molecular device,

Inputs		Outputs	
Hg^{2+}	His	I_{545nm}	I_{460nm}/I_{545nm}
I_1	I_2	O_1	O_2
0	0	0	0 (<1)
0	1	0	0 (<1)
1	0	0	1 (~60)
1	1	1	0 (<1)

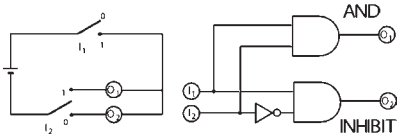

Figure 7. Truth table and representation of the electronic circuit (top) and combinational logic scheme (bottom) of **AND** and **INHIBIT** logic operations.

such as a logic gate. Interestingly, as shown in Figure 7, two-input **AND** and **INHIBIT** gates were successfully fabricated for $[Ir(ppy)_2(PBT)]$. Herein, Hg^{2+} (input 1, denoted as I_1, 2.0 equiv, binary 1; 0 equiv, binary 0), and histidine (input 2, denoted as I_2, 5.0 equiv, binary 1; 0 equiv, binary 0) were used as these inputs, and the emission intensities at 460 nm ($I_{460\ nm}$, corresponding to the PBT emission) and 545 nm ($I_{545\ nm}$, corresponding to the isoemissive point, output 1, denoted as O_1) and the values of the ratio $I_{460\ nm}/I_{545\ nm}$ (output 2, denoted as O_2) were taken as the outputs of the system. As shown in Figure 7, the $I_{545\ nm}$ (O_1) was distinctly high (logic 1) only when both inputs (I_1, I_2) were high (1, 1), and the output was low (logic 0) when either or both of the inputs (I_1, I_2) were low [(0, 0) or (0, 1) or (1, 0)]. The experimental truth table for this device summarizes the input−output response and confirms that $[Ir(ppy)_2(PBT)]$ behaves as an **AND** logic gate. Thus, a two-input **AND** gate was fabricated by using Hg^{2+} and histidine as inputs and taking $I_{545\ nm}$ (O_1) as the output. Furthermore, we also fabricated an **INHIBIT** logic gate by using Hg^{2+} (I_1) and histidine (I_2) as two inputs and taking the ratio $I_{460\ nm}/I_{545\ nm}$ (O_2) as the output (Figure 7). In this device, $I_{460\ nm}/I_{545\ nm}$ (O_2) is distinctly high (logic 1) when (I_1, I_2) is (1, 0), indicating that Hg^{2+} and histidine modulate $I_{460\ nm}/I_{545\ nm}$ (O_2) through an **INHIBIT** logic operation. Therefore, two-input **AND** and **INHIBIT** gates were successfully fabricated for $[Ir(ppy)_2(PBT)]$ by using chemical inputs and taking the luminescent emission signals as outputs. Of course, it should be noted that the logic gate in solution described in this work is not practicable.

CONCLUSIONS

In summary, we have demonstrated for the first time that two neutral complexes, $[Ir(ppy)_2(PBT)]$ and $[Ir(ppy)_2(PBO)]$, containing different N^O ligands can serve as logic gates. Theoretical calculations and detailed studies of the photophysical and electrochemical properties have shown that the N^O ligands dominate the emission properties of these two complexes. Furthermore, the complex $[Ir(ppy)_2(PBT)]$ containing an S atom in the N^O ligand can serve as a highly selective chemodosimeter for Hg^{2+}, permitting ratiometric and naked-eye detection. More importantly, $[Ir(ppy)_2(PBT)]$ has been further developed as **AND** and **INHIBIT** logic gates by using Hg^{2+} (I_1) and histidine (I_2) as two inputs and the phosphorescence signal as the output. This preliminary understanding of the sensing mechanism can be expected to help the design of new

dx.doi.org/10.1021/ic102481x |*Inorg. Chem.* 2011, 50, 5969–5977

phosphorescent probes based on iridium(III) complexes by simply modifying the ligands to contain specific coordinating elements, allowing further exploration of this new application of phosphorescent iridium(III) complexes in molecular logic gates.

■ ASSOCIATED CONTENT

Supporting Information. The ^{1}H NMR, ESI-MS, selected bond distances and angles, calculated energy levels of the lower lying transtions, absorption and luminescence spectra of $Ir(ppy)_2(PBT)$ and $Ir(ppy)_2(PBO)$, changes in the ^{1}H NMR, ESI-MS, absorption and luminescence spectra of $Ir(ppy)_2(PBT)$ and PBT in THF/H_2O solution with Hg^{2+}. This material is available free of charge via the Internet at http://pubs.acs.org.

■ AUTHOR INFORMATION

Corresponding Author

*Fax: 86-21-55664621. Phone: 86-21-55664185. E-mail: fyli@fudan.edu.cn.

■ ACKNOWLEDGMENT

The authors thank National Natural Science Funds for Distinguished Young Scholars (20825101), National Natural Science Foundation of China (91027004, 50803028 and 20804019), Shanghai Sci. Tech. Comm. (10431903100), IRT0911, Shanghai Leading Academic Discipline Project (B108) for financial support.

■ REFERENCES

(1) (a) Chi, Y.; Chou, P. T. *Chem. Soc. Rev.* **2010**, *39*, 638–655. (b) Chen, Z. Q.; Bian, Z. Q.; Huang, C. H. *Adv. Mater.* **2010**, *22*, 1534–1539. (c) Wong, W. Y.; Ho, C. L. *Coord. Chem. Rev.* **2009**, *253*, 1709–1758. (d) You, Y.; Park, S. Y. *Dalton Trans.* **2009**, *8*, 1267–1282. (e) Ulbricht, C.; Beyer, B.; Friebe, C.; Winter, A.; Schubert, U. S. *Adv. Mater.* **2009**, *21*, 4418–4441. (f) Tan, W. J.; Zhang, Q.; Zhang, J. J.; Tian, H. *Org. Lett.* **2009**, *11*, 161–176. (g) Wong, W. Y.; Ho, C. L. *J. Mater. Chem.* **2009**, *19*, 4457–4482.

(2) (a) Baldo, M. A.; Thompson, M. E.; Forrest, S. R. *Nature* **2000**, *403*, 750–753. (b) Reineke, S.; Lindner, F.; Schwartz, G.; Seidler, N.; Walzer, K.; Lüssem, B.; Leo, K. *Nature* **2009**, *459*, 234–238. (c) Wu, C.; Chen, H. F.; Wong, K. T.; Thompson, M. E. *J. Am. Chem. Soc.* **2010**, *132*, 3133–3139. (d) Chen, K.; Yang, C. H.; Chi, Y.; Liu, C. S.; Chang, C. H.; Chen, C. C.; Wu, C. C.; Chung, M. W.; Cheng, Y. M.; Lee, G. H.; Chou, P. T. *Chem.—Eur. J.* **2010**, *16*, 4315–4327. (e) Wong, W. Y.; Ho, C. L.; Gao, Z. Q.; Mi, B. X.; Chen, C. H.; Cheah, K. W.; Lin, Z. *Angew. Chem., Int. Ed.* **2007**, *46*, 1558–1558. (f) Bian, Z. Q.; Huang, C. H. *Highly Efficient OLEDs with Phosphorescent Materials*; Wiley-VCH Verlag GmbH & Co. KgaA: Weinheim, Germany, 2008; pp 391−420.

(3) (a) Su, H. C.; Fang, F. C.; Hwu, T. Y.; Hsieh, H. H.; Chen, H. F.; Lee, G. H.; Peng, S. M.; Wong, K. T.; Wu, C. C. *Adv. Funct. Mater.* **2007**, *17*, 1019–1027. (b) Mydlak, M.; Bizzarri, C.; Hartmann, D.; Sarfert, W.; Schmid, G.; De Cola, L. *Adv. Funct. Mater.* **2010**, *20*, 1812–1820.

(4) Recent review: Zhao, Q.; Li, F. Y.; Huang, C. H. *Chem. Soc. Rev.* **2010**, *39*, 3007–3030, and some references therein.

(5) Review: (a) Lo, K. K. W.; Hui, W. K.; Chung, C. K.; Tsang, K. H. K.; Lee, T. K. M.; Li, C. K.; Lau, J. S. Y.; Ng, D. C. M. *Coord. Chem. Rev.* **2006**, *250*, 1724–1736. (b) Lo, K. K. W.; Tsang, K. H. K.; Sze, K. S.; Chung, C. K.; Lee, T. K. M.; Zhang, K. Y.; Hui, W. K.; Li, C. K.; Lau, J. S. Y.; Ng, D. C. M.; Zhu, N. *Coord. Chem. Rev.* **2007**, *251*, 2292–2310.

(6) (a) Ma, D. L.; Wong, W. L.; Chung, W. H.; Chan, F. Y.; So, P. K.; Lai, T. S.; Zhou, Z. Y.; Leung, Y. C.; Wong, K. Y. *Angew. Chem., Int. Ed.* **2008**, *47*, 3735–3739. (b) Leung, M. C. L.; Wong, K. M. C.; Tsang, Y. K. T.; Yam, V. W. W. *Chem. Commun.* **2010**, *46*, 7709–7711.

(7) Recent reviews: (a) Moreira, V. F.; Greenwood, F. L. T.; Coogan, M. P. *Chem. Commun.* **2010**, *46*, 186. (b) Zhao, Q.; Li, F. Y.; Huang, C. H. *Chem. Soc. Rev.* **2011**, *40*, 2508−2524; and some references therein.

(8) Murphy, L.; Congreve, A.; Pålsson, L. O.; Williams, J. A. G. *Chem. Commun.* **2010**, *46*, 8743–8745.

(9) (a) Zhao, Q.; Liu, S. J.; Shi, M.; Li, F. Y.; Yi, T.; Huang, H. C. *Organometallics* **2007**, *26*, 5922–5930. (b) Zhao, Q.; Li, F. Y.; Liu, S. J.; Yu, M. X.; Liu, Z. Q.; Yi, T.; Huang, C. H. *Inorg. Chem.* **2008**, *47*, 9256–9264. (c) You, Y.; Park, S. Y. *Adv. Mater.* **2008**, *20*, 3820–3826. (d) Xu, W. J.; Liu, S. J.; Zhao, X. Y.; Sun, S.; Cheng, S.; Ma, T. C.; Sun, H. B.; Zhao, Q.; Huang, W. *Chem.—Eur. J.* **2010**, *16*, 7125–7133.

(10) (a) Ho, M. L.; Hwang, F. M.; Chen, P. N.; Hu, Y. H.; Cheng, Y. M.; Chen, K. S.; Lee, G. H.; Chi, Y.; Chou, P. T. *Org. Biomol. Chem.* **2006**, *4*, 98–103. (b) Zhao, Q.; Cao, T. Y.; Li, F. Y.; Li, X. H.; Jing, H.; Yi, T.; Huang, C. H. *Organometallics* **2007**, *26*, 2077–2081. (c) Zhao, Q.; Liu, S. J.; Li, F. Y.; Yi, T.; Huang, C. H. *Dalton Trans.* **2008**, *29*, 3836–3840. (d) Shi, H. F.; Liu, S. J.; Sun, H. B.; Xu, W. J.; An, Z. F.; Chen, J.; Sun, S.; Lu, X. M.; Zhao, Q.; Huang, W. *Chem.—Eur. J.* **2010**, *16*, 12158–12167.

(11) (a) Chen, H. L.; Zhao, Q.; Wu, Y. B.; Li, F. Y.; Yang, H.; Yi, T.; Huang, C. H. *Inorg. Chem.* **2007**, *46*, 11075–11081. (b) Xiong, L. Q.; Zhao, Q.; Chen, H. L.; Wu., Y. B.; Dong, Z. S.; Zhou, Z. G.; Li, F. Y. *Inorg. Chem.* **2010**, *49*, 6402–6408.

(12) (a) Lo, K. K. W.; Tsang, K. H. K.; Sze, K. S.; Chung, C. K.; Lee, T. K. M.; Zhang, K. Y.; Hui, W. K.; Li, C. K.; Lau, J. S. Y.; Ng, D. C. M.; Zhu, N. *Coord. Chem. Rev.* **2007**, *251*, 2292–2310. (b) Pruszynski, M.; Bilewicz, A.; Zalutsky, M. R. *Bioconjugate Chem.* **2008**, *19*, 958–965. (c) Zhang, K. Y.; Lo, K. K. W. *Inorg. Chem.* **2009**, *48*, 6011–6025.

(13) (a) Li, S. P. Y.; Liu, H. W.; Zhang, K. Y.; Lo, K. K. W. *Chem.—Eur. J.* **2010**, *16*, 8329–8339. (b) Zhang, K. Y.; Li, S. P. Y.; Zhu, N.; Or, I. W. S.; Cheung, M. S. H.; Lam, Y. W.; Lo, K. K. W. *Inorg. Chem.* **2010**, *49*, 2530–2540. (c) Leung, S. K.; Kwok, K. Y.; Zhang, K. Y.; Lo, K. K. W. *Inorg. Chem.* **2010**, *49*, 4984–4995. (d) Zhang, K. Y.; Liu, H. W.; Fong, T. T. H.; Chen, X. G.; Lo, K. K. W. *Inorg. Chem.* **2010**, *49*, 5432–5443. (e) Liu, H. W.; Zhang, K. Y.; Law, W. H. T.; Lo, K. K. W. *Organometallics* **2010**, *29*, 3474–3476. (f) Zhang, K. Y.; Lo, K. K. W. *Inorg. Chem.* **2009**, *48*, 6011–6025. (g) Lau, J. S. Y.; Lee, P. K.; Tsang, K. H. K.; Ng, C. H. C.; Lam, Y. W.; Cheng, S. H.; Lo, K. K. W. *Inorg. Chem.* **2009**, *48*, 708–718.

(14) (a) Yu, M. X.; Zhao, Q.; Shi, L. X.; Li, F. Y.; Zhou, Z. G.; Yang, H.; Yi, T.; Huang, C. H. *Chem. Commun.* **2008**, 2115–2117. (b) Zhao, Q.; Yu, M. X.; Shi, L. X.; Liu, S. J.; Li, C. Y.; Shi, M.; Zhou, Z. G.; Huang, C. H.; Li., F. Y. *Organometallics* **2010**, *29*, 1085–1091. (c) Jiang, W.; Gao, Y.; Sun, Y.; Ding, F.; Xu, Y.; Bian, Z. Q.; Li, F. Y.; Bian, J.; Huang, C. H. *Inorg. Chem.* **2010**, *49*, 3252–3260. (d) Wu, H. Z.; Yang, T. S.; Zhao, Q.; Zhou, J.; Li, C. Y.; Li, F. Y. *Dalton Trans.* **2011**, *40*, 1969–1976.

(15) (a) Tian, H.; Wang, Q. C. *Chem. Soc. Rev.* **2006**, *35*, 361–374. (b) Qu, D. H.; Ji, F. Y.; Wang, Q.; Tian, H. *Adv. Mater.* **2006**, *18*, 2035–2038. (c) Guo, Z. Q.; Zhu, W. H.; Shen, L. J.; Tian, H. *Angew. Chem., Int. Ed.* **2007**, *46*, 5549–5553.

(16) (a) Uchiyama, S.; Kawai, N.; De Silva, A. P.; Iwai, K. *J. Am. Chem. Soc.* **2004**, *126*, 3032–3033. (b) Wang, C.; Zhang, D. Q.; Zhuang, G. X.; Xiang, J. F.; Zhu, D. B. *Chem.—Eur. J.* **2008**, *14*, 5680–5686. (c) García-Acosta, B.; Martínez-Máñez, R.; Sancenón, F.; Soto, J.; Rurack, K.; Spieles, M.; García-Breijo, E.; Gil, L. *Inorg. Chem.* **2007**, *46*, 3123–3135. (d) Broomsgrove, A. E. J.; Addy, D. A.; Di Paolo, A.; Morgan, I. R.; Bresner, C.; Chislett, V.; Fallis, I. A.; Thompson, A. L.; Vidovic, D.; Aldridge, S. *Inorg. Chem.* **2010**, *49*, 157–173.

(17) Frisch, M. J.; Trucks, G. W.; Schlegel, H. B.; Scuseria, G. E.; Robb, M. A.; Cheeseman, J. R.; Montgomery, J. A., Jr.; Vreven, T.; Kudin, K. N.; Burant, J. C.; Millam, J. M.; Iyengar, S. S.; Tomasi, J.; Barone, V.; Mennucci, B.; Cossi, M.; Scalmani, G.; Rega, N.; Petersson, G. A.; Nakatsuji, H.; Hada, M.; Ehara, M.; Toyota, K.; Fukuda, R.; Hasegawa, J.; Ishida, M.; Nakajima, T.; Honda, Y.; Kitao, O.; Nakai, H.; Klene, M.; Li, X.; Knox, J. E.; Hratchian, H. P.; Cross, J. B.; Bakken, V.; Adamo, C.; Jaramillo, J.; Gomperts, R.; Stratmann, R. E.; Yazyev, O.;

Austin, A. J.; Cammi, R.; Pomelli, C.; Ochterski, J. W.; Ayala, P. Y.; Morokuma, K.; Voth, G. A.; Salvador, P.; Dannenberg, J. J.; Zakrzewski, V. G.; Dapprich, S.; Daniels, A. D.; Strain, M. C.; Farkas, O.; Malick, D. K.; Rabuck, A. D.; Raghavachari, K.; Foresman, J. B.; Ortiz, J. V.; Cui, Q.; Baboul, A. G.; Clifford, S.; Cioslowski, J.; Stefanov, B. B.; Liu, G.; Liashenko, A.; Piskorz, P.; Komaromi, I.; Martin, R. L.; Fox, D. J.; Keith, T.; Al-Laham, M. A.; Peng, C. Y.; Nanayakkara, A.; Challacombe, M.; Gill, P. M. W.; Johnson, B.; Chen, W.; Wong, M. W.; Gonzalez, C.; Pople, J. A. *Gaussian 03*, revision C.02; Gaussian, Inc.: Wallingford, CT, 2004.

(18) Nonoyama, K. *Bull. Chem. Soc. Jpn.* **1974**, *47*, 467–468.

(19) Neve, F.; Deda, M. L.; Crispini, A.; Bellusci, A.; Puntoriero, F.; Campagna, S. *Organometallics* **2004**, *23*, 5856–5863.

(20) Thomas, K. R. J.; Velusamy, M.; Lin, J. T.; Chien, C. H.; Tao, Y. T.; Wen, Y. S.; Hu, Y. H.; Chou, P. T. *Inorg. Chem.* **2005**, *44*, 5677–5685.

(21) Okada, S.; Okinaka, K.; Iwawaki, H.; Furugori, M.; Hashimoto, M.; Mukaide, T.; Kamatani, J.; Igawa, S.; Tsuboyama, A.; Takiguchi, T.; Ueno, K. *Dalton Trans.* **2005**, *9*, 1583–1590.

(22) (a) Li, M. J.; Ko, C. C.; Duan, G. P.; Zhu, N. Y.; Yam, V. W. W. *Organometallics* **2007**, *26*, 6091–6098. (b) Coronado, E.; Galan-Mascaros, J. R.; Marti-Gastaldo, C.; Palomares, E. J.; Durrant, R. R.; Vilar, R.; Gratzel, M.; Nazeeruddin, Md. K. *J. Am. Chem. Soc.* **2005**, *127*, 12351–12356.

(23) Pearson, R. G. *J. Am. Chem. Soc.* **1963**, *85*, 3533–3543.